Received: 21 February 2020 | Revised: 11 May 2020 | Accepted: 19 May 2020
DOI: 10.1002/pip.3301

RESEARCH ARTICLE

PROGRESS IN PHOTOVOLTAICS WILEY

Organic tandem solar cells under indoor light illumination

Swarup Biswas[1] | Young-Jun You[2] | Premkumar Vincent[3] | Jin-Hyuk Bae[3] | Jae Won Shim[4] | Hyeok Kim[1]

[1]School of Electrical and Computer Engineering, Institute of Information Technology, University of Seoul, 163 Seoulsiripdaero, Dongdaemun-gu, Seoul, 02504, Republic of Korea

[2]Division of Electronics and Electrical Engineering, Dongguk University, Seoul, 04620, Republic of Korea

[3]School of Electronics Engineering, Kyungpook National University, 80 Daehakro, Bukgu, Daegu, 41566, Republic of Korea

[4]School of Electrical Engineering, Korea University, 145 Anam-ro, Seongbuk-gu, Seoul, 02841, Republic of Korea

Correspondence

J. H. Bae, School of Electronics Engineering, Kyungpook National University, 80 Daehakro, Bukgu, Daegu, Republic of Korea.
Email: jhbae@ee.knu.ac.kr

J. W. Shim, School of Electrical Engineering, Korea University, 145 Anam-ro, Seongbuk-gu, Seoul 02841, Republic of Korea.
Email: jwshim19@korea.ac.kr

H. Kim, School of Electrical and Computer Engineering, Institute of Information Technology, University of Seoul, 163 Seoulsiripdaero, Dongdaemun-gu, Seoul 02504, Republic of Korea.
Email: hyeok.kim@uos.ac.kr

Funding information

Ministry of Education, Grant/Award Number: NRF-2018R1D1A1B07043759/NRF-2018 R1D1A3B07049992; Ministry of Science, ICT & Future Planning, Grant/Award Number: NRF-2016M1A2A2940912; Ministry of Science and ICT, Grant/Award Number: 2018R1A2B6008815

Abstract

The lifetime of a device depends highly on that of its battery. In order to enhance the longevity of microsystems or sensor networks, it is necessary for these devices to be self-powered. Indoor photovoltaics allow the possibility of harvesting artificial light sources for powering microsystems. Whereas indoor photovoltaics based on single active layers have showed high efficiencies under LED lighting, tandem structures have yet to be tested extensively. In our study, we use finite-difference time-domain simulations to study the highest possible short-circuit current density that can be extracted from tandem organic devices. We compare the simulation results to the results for photovoltaic devices based on single bulk active layer heterojunctions. Our simulations found that although detailed balanced band gap calculations show tandem photovoltaics to be viable, the low-intensity emission spectra of white LED light sources can be better harvested by single active layer-based photovoltaics. The current-matching limitation of a tandem photovoltaic structure connected in series limits the highest output current and open-circuit voltage of the device and, thus, its performance for the illumination of lower intensity light.

KEYWORDS

artificial light harvesting, finite-difference time domain, indoor photovoltaic, tandem

1 | INTRODUCTION

Solar cells have been researched extensively for the past few decades. While there has been good progress in achieving high efficiencies using single band gap photovoltaic (PV) systems, we have almost reached the theoretical maximum achievable efficiency set by the Shockley–Queisser limit.[1,2] There are a few companies that have exhibited single-cell efficiencies close to the theoretical maximum achievable efficiency under 1 sun.[3–8] In order to absorb a larger part of the illumination spectrum, researchers have developed tandem, multiacceptor, and donor active layer structures.[9,10] Among them, tandem solar cells, which have already crossed the Shockley–Queisser

Swarup Biswas, Young-Jun You, and Premkumar Vincent contributed equally to this work.

limit, are easier to configure as they consist of two or more separate subcells that absorb different portions of the incoming light spectrum. In the series configuration, the short-circuit current density (J_{SC}) of a tandem solar cell is limited by the minimum J_{SC} among the subcells. Thus, it is important to select the subcell band gaps accordingly such that the absorption bands do not overlap. Tandem solar cells have been calculated to reach efficiencies as high as 85%–86% under 1 sun for ideal, theoretical unconstrained stack systems. Practically, tandem solar cells constructed through band gap optimization have already crossed the efficiency level of over 40% under 1-sun condition.[11] Meanwhile, indoor PVs are gaining popularity as components of microenergyharvesting systems owing to the growing demand for utilizing ambient energy. Indoor PV can be used to power wireless sensor nodes, self-powering devices, and so forth.[12–15] Till now, PV devices based on different materials such as silicone,[16] organic semiconductors,[17] III–V semiconductors,[18] sensitized dyes,[19] copper indium gallium selenide (CIGS),[20] and perovskites[21] have been tested extensively for indoor applications. Among them, the organic PV cell is one of the best performing PV cells owing to its excellent spectral match with indoor light sources. Indoor light, one of the main sources of ambient energy, consists of artificial lighting and sunlight illuminating the room through windows. There are several artificial light sources that have spectrum peaks at different wavelengths.[22,23] While white LED light sources peak at ~450 nm and ~550 nm wavelengths, fluorescent tube light sources have additional peaks at ~400 nm and ~600nm wavelengths. The emission spectrum of sodium lamp light sources is concentrated near the 600nm wavelength, while incandescent lamps have high spectral emission at wavelengths greater than 600 nm. Therefore, an indoor PV cell with the ability to absorb a larger part of the illumination spectrum is highly desired. In this case, tandem PV cells may be good options, as they already exhibit better performance than single-cell configurations under the 1-sun condition. Up to now, very few attempts have been made to construct tandem PV cells for operation under indoor light illumination. Therefore, a proper investigation on the construction and performance level of tandem PV cells for indoor applications is highly desirable. In this regard, a study combining experimental and optical simulations can be a very useful tool to investigate the performance level of tandem PV cells as a function of different parameters, characterizing the nature of factors such as the cells, illuminating light, and semiconductors involved.[24]

Therefore, in this work, we first constructed a tandem PV cell structure (Figure 1A) with P3HT:ICBA as the active layer for the front subcell and PTB7:$PC_{70}BM$ as the active layer for the back subcell. We also constructed PV cells in the single-cell configuration using each of the two active materials. The devices were then tested under 1-sun and indoor light illumination. To better understand the performance variation of different PV cells with various configurations under different illumination conditions, we performed a simulation study on the tandem PV cell with a MEH-PPV:$PC_{60}BM$-based cell as the front subcell and a PCPDTBT: $PC_{70}BM$-based cell as the back subcell to investigate its performance level in indoor light environment, as these two active materials have optimized band gaps for white LED light illumination. We then compared the maximum absorption efficiency of the tandem PV structure with the single bulk heterojunction (BHJ) structure under white LED lighting. In the device simulation study, we used finite-difference time-domain method (FDTD) optical modeling to obtain the ideal short-circuit current density ($J_{SC,ideal}$) that can be derived from the optimum tandem structure obtained from the previous calculations.

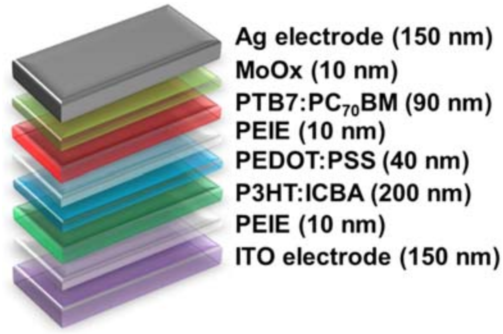

FIGURE 1 Conventional tandem PV device structure, which exhibits good outdoor performance but very poor indoor performance [Colour figure can be viewed at wileyonlinelibrary.com]

2 | EXPERIMENTAL SECTION

2.1 | Materials

Polyethylenimine ethoxylated (PEIE), 2-methoxyethanol, 1,8-diiodooctane, dichlorobenzene (DCB), and chlorobenzene (CB) were purchased from Sigma-Aldrich and used without any further purification. Poly[[4,8-bis[(2-ethylhexyl)oxy]benzo[1,2-b:4,5-b′] dithiophene-2,6-diyl][3-fluoro-2-[(2-ethylhexyl)carbonyl]thieno[3,4-b] thiophenediyl]] (PTB7) was obtained from one material. The compound [6,6]-Phenyl-C71-butyric acid methyl ester ($PC_{70}BM$) was provided by nano-c. Poly(3-hexylthiophene) (P3HT) and indene-C60 bisadduct (ICBA) were purchased from Rieke Metals Inc. and Luminescence Technology Corp., respectively.

2.2 | Solution preparation

PEIE (0.1 wt.%) was mixed with 2-methoxyethanol and stirred (1000 rpm) for 12 h in ambient air at room temperature; meanwhile, 20-mg P3HT and 20mg ICBA were mixed in 1ml DCB and stirred (1000 rpm) for 12 h at 70°C inside a N_2filled glove box (GB). Then, 10mg PTB7 and 15mg $PC_{70}BM$ were added to a mixture of 970μl CB and 30μl 1,8-diiodooctane and stirred (1000 rpm) for 12 h at room temperature inside the N_2filled GB.

2.3 | Device fabrication

To fabricate the tandem PV device (Figure 1), the glass substrate was first coated with indium tin oxide (sheet resistivity ~10 Ω/sq) and washed carefully using standard methods. The substrates were then immersed within liquid detergent, ultrasonicated for 30 min, and rinsed with deionized (DI) water. The substrates were next cleaned with DI water, acetone, and 2-propanol sequentially. Finally, the substrates were dried by blowing N_2 gas. After cleaning the substrates, we formed 10-nm PEIE films on the substrates through the spin coating of filtrated (through 0.2-μm-pore PTFE filter) PEIE solution at 5000 rpm in a normal atmosphere. The PEIE-coated substrates were then dried on a hot plate for 10 min at 110°C and were transferred inside the GB. The P3HT:ICBA solution was next spin-coated on the PEIE-coated substrate at 800 rpm for 30 s, and the solvent from the P3HT:ICBA film was removed through annealing at 70°C for 8 h. Thereafter, the solvent-free P3HT:ICBA film was annealed at 150°C for 10 min, while 40-nm PEDOT:PSS film was formed onto the P3HT:ICBA film through spin coating of PEDOT:PSS solution at 5000 rpm for 60 s. The film was then dried through heating at 100°C for 10 min. PEIE was again coated onto the PEDOT:PSS surface by following the same protocol, and subsequently, PTB7:PC_{70}BM (90 ± 5 nm) was spin-coated onto the PEIE surface at 1000 rpm for 20 s. After removing all the solvent from the PTB7:PC_{70}BM film, MoO_x (10 nm) was deposited through a shadow mask onto the PTB7:PC_{70}BM layers using a Daedong High Tech (Republic of Korea) vacuum thermal evaporation system, which was directly attached to the GB. The deposition rate was fixed at 0.1–0.15 nm/s, and the base pressure was maintained at approximately 6 μPa. Finally, a 150-nm-thick Ag layer was formed within the vacuum thermal depositor system at a deposition rate of 0.1–0.2 nm/s. For comparison, we also fabricated PV cells with only P3HT:ICBA (ITO/PEIE/P3HT:ICBA/MoO_x/Ag) or PTB7:PC_{70}BM (ITO/PEIE/PTB7:PC_{70}BM/MoO_x/Ag) as the active layers. The coating procedures of the two active layer materials were the same as those for the tandem PV cell.

2.4 | Device characterization

We used a Keithley 2401 source meter operated by the K730 program developed by McScience, Republic of Korea, to record the current density–voltage (*J-V*) characteristics of different PV devices under both dark and illuminated conditions. For the PV device characterization, we used a Xe55AM1.5 G (100 mW/cm^2) solar simulator. The LED (indoor) light simulation system was provided by McScience, Republic of Korea, with a COB LED white LED lamp.

2.5 | Simulation procedure

FDTD simulations were carried out using Lumerical, FDTD solutions software. A plane wave source was used as the illumination source in order to simulate 500 lx and 1000 lx LED light sources. We mentioned earlier that band gap optimization is essential for multi-junction structures. Therefore, we estimated the optimum band gap for the two subcells in a monolithic tandem PV cell operating under LED lamp illumination of LED lamp by employing Equation 1)[23]:

$$PCE_{max} = \frac{(E_{g1} + E_{g1}).\min\left(\int_{E_{g1}}^{\infty} N(E)dE,\ \int_{E_{g2}}^{E_{g1}} N(E)dE\right)}{\int_{0}^{\infty} E.N(E)dE},\ \text{while}\ \ E_{g1} > E_{g2}, \tag{1}$$

where PCE_{max} is the maximum power conversion efficiency, E_{g1} and E_{g2} are the band gaps of the front and back subcells, respectively, and *N*(*E*) is the incident photon flux. The complex refractive indices for the solar cell materials were taken from experiments and other papers.[25] The structures of the tandem solar cells to be optimized by FDTD simulation were sketched using the TCAD tool in the simulation software. The device structures are shown in Figure 3A–C. A common assumption in optical simulations is to use 100% internal quantum efficiency (IQE) in order to obtain the maximum ideal short-circuit current density ($J_{SC,ideal}$). The 2D FDTD simulation was carried out by following the procedure detailed in our previous study.[25–27] Periodic boundary conditions were used along the plane perpendicular to the device structure, and perfectly matched layers were used along the device growth direction.

3 | RESULTS AND DISCUSSION

Recently, Chen et al. successfully fabricated a tandem PV cell structure (Figure 1) with P3HT:ICBA as the active layer for the front subcell and PTB7:PC_{70}BM as the active layer for the back subcell, and they tested the device under the 1-sun condition.[28] They observed that the tandem PV cell has a higher efficiency for converting light energy into electrical energy than single-cell configurations with the constituent active materials. Here, in this work, we reconstructed the tandem PV structure with the same active materials and also constructed PV cells (single-cell configuration) by using all the active layers individually. We subsequently tested the performance of the conventional structures under both outdoor and indoor light (500 lx and 1000 lx white LED) conditions. Experimental results for different PV devices (tandem and single-cell configuration) operated under 1-sun and indoor light (white LED) conditions are presented in Tables 1 and 2, respectively. From Table 1, it can be observed that the tandem stuctured PV devices exhibit better power conversion efficiency (PCE)

TABLE 1 Experimentally obtained data (averaged over five devices) for different PV devices operated under AM1.5 G illumination

Device	Active material	V_{OC} (mV)	J_{SC} (mA/cm^2)	FF (%)	PCE (%)	R_S (Ω × cm^2)
Tandem	P3HT:ICBA and PTB7:PC_{70}BM	1526 ± 7	8.3 ± 0.0	60.9 ± 0.4	7.7 ± 0.0	38 ± 0.0
Single-celled	P3HT:ICBA	828 ± 1	9.8 ± 0.2	60.4 ± 1.2	4.9 ± 0.2	17 ± 1
	PTB7:PC_{70}BM	715 ± 5	14.8 ± 0.3	50.7 ± 1.2	5.4 ± 0.3	10 ± 1

TABLE 2 Experimentally extracted data (averaged over five devices) of different PV devices operated under white LED illumination

Device	Active material	Luminance (lx)	P_{in} (μW/cm^2)	V_{OC} (mV)	J_{SC} (μA/cm^2)	FF (%)	PCE (%)	MPD (μW/cm^2)	R_{SH} (Ω × cm^2)
Tandem	P3HT:ICBA and PTB7: $PC_{70}BM$	500	170	663 ± 48	29.7 ± 2.8	53.6 ± 13.4	6.4 ± 2.3	10.9 ± 3.9	$1.9 \times 10^5 \pm 3.5 \times 10^3$
		1000	280	707 ± 33	58.3 ± 5.6	56.8 ± 9.8	8.5 ± 3.7	23.8 ± 6.4	$1.2 \times 10^5 \pm 2.0 \times 10^3$
Single-celled	P3HT:ICBA	500	170	675 ± 35	37.5 ± 1.7	64.0 ± 8.2	9.8 ± 0.0	16.7 ± 3.5	$1.3 \times 10^5 \pm 1.4 \times 10^3$
		1000	280	686 ± 15	72.5 ± 3.2	54.0 ± 12.6	9.6 ± 2.2	26.8 ± 6.2	$1.1 \times 10^5 \pm 1.3 \times 10^3$
	PTB7: $PC_{70}BM$	500	170	487 ± 50	43.0 ± 1.3	44.2 ± 8.5	5.5 ± 1.5	9.4 ± 2.5	$2.9 \times 10^5 \pm 2.5 \times 10^3$
		1000	280	537 ± 52	95.3 ± 2.9	47.2 ± 6.0	8.7 ± 1.7	22.0 ± 4.3	$2.1 \times 10^5 \pm 1.5 \times 10^3$

compared with their single-cell PV structure counterparts under 1-sun condition; however, the behavior of the tandem PV cells changed when we tested the devices under white LED illumination (i.e., indoor light). The data (Table 2) of the characteristics of the different PV cells tested under white LED light illumination (500 lx and 1000 lx) indicate that the tandem-structured PV cells have lower PCE than that of the single-cell PV cells. The PCE of a PV cell can be expressed by the Equation 2).

$$PCE(\%) = \frac{J_{SC} * V_{OC} * FF}{P_{in}}. \tag{2}$$

From the expression, it can be noted that, the PCE value of a PV device is dependent on the short-circuit current density (J_{SC}), open-circuit voltage (V_{OC}), and fill factor (FF) of the cell. Figure 2 clearly shows that the J_{SC} of the tandem PV cell is always less than that of the single bulk heterogeneous PV cell. The reason behind this phenomenon is further investigated by simulations to be described later. Meanwhile, Figure 2A shows that the V_{OC} value of the tandem cell is very high (near the sum of the V_{OC} values of the single bulk heterogeneous PV cells) for 1-sun condition (outdoor light); however, when the intensity of the incident light decreases (illumination of white LED lamp), the V_{OC} value of the tandem cell becomes nearly the same as the V_{OC} value of the single-celled PV structure (Figure 2B). Therefore, the PCE value of the tandem PV device under the illumination of white LED light becomes smaller than those of the single bulk heterogeneous PV cells constructed by the active materials used in the tandem PV cell. It is not possible to establish an appropriate conclusion on the basis of only a single experimental result. There are different variables, such as band gap matching and thickness of the different active layers, that should be considered. For this reason, we performed a detailed PV device simulation study using FDTD solutions software. In the experimental study, we used P3HT:ICBA and PTB7: $PC_{70}BM$ as the active layers of the front and back subcells, respectively. Their band gaps are appropriate for outdoor light. The ideal band gaps (calculated from Equation 1) for the active layers of the front and back subcells of a tandem PV cell operating under white LED illumination are 2.338 and 1.833 eV, respectively. We found that, MEH-PPV:$PC_{60}BM$ had a band gap of 2.3 eV and PCPDTBT:$PC_{70}BM$ had a band gap of 1.8 eV. Therefore, these two materials were chosen for the front and back subcells, respectively, in our device simulation study. The tandem PV structure optimized for white LED illumination (Figure 3A) was constructed with ITO (150 nm)/PEDOT:PSS (50 nm)/MEH-PPV:$PC_{60}BM$/LiF (5 nm)/PH1000 (40 nm)/PEDOT:PSS (50 nm)/PCPDTBT:$PC_{70}BM$/Ca (20 nm)/Al (100 nm). The FDTD simulations were subsequently performed under 500lx white LED and 1000lx white LED illumination. For comparison, we also constructed single-celled PV structures with MEH-PPV:$PC_{60}BM$ (Figure 3B) and PCPDTBT:$PC_{70}BM$ (Figure 3C) as the active layers. The $J_{SC,ideal}$ of the tandem structure obtained from the simulation is presented in Figure 4A,B. The $J_{SC,ideal}$ of a monolithic tandem structure, such as the

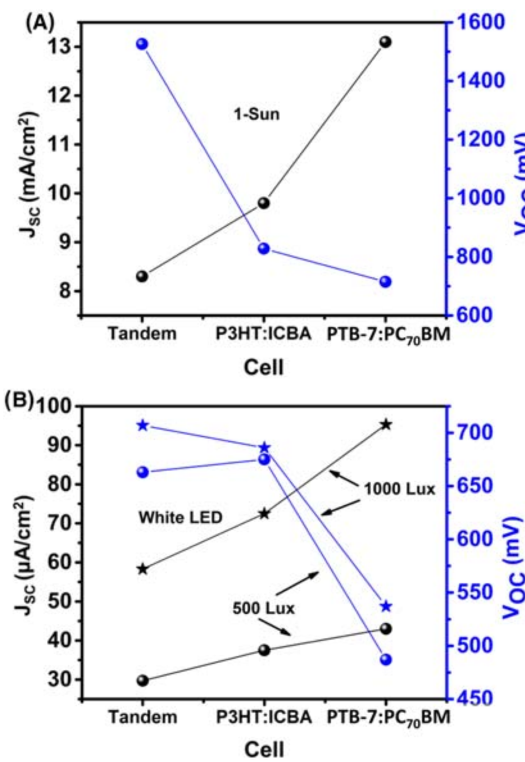

FIGURE 2 Short-circuit current density (J_{SC}) and open-circuit voltage (V_{OC}) of different PV devices operating under the illumination of (A) outdoor light (1-sun condition) and (B) white LED light (500 lx and 1000 lx) [Colour figure can be viewed at wileyonlinelibrary.com]

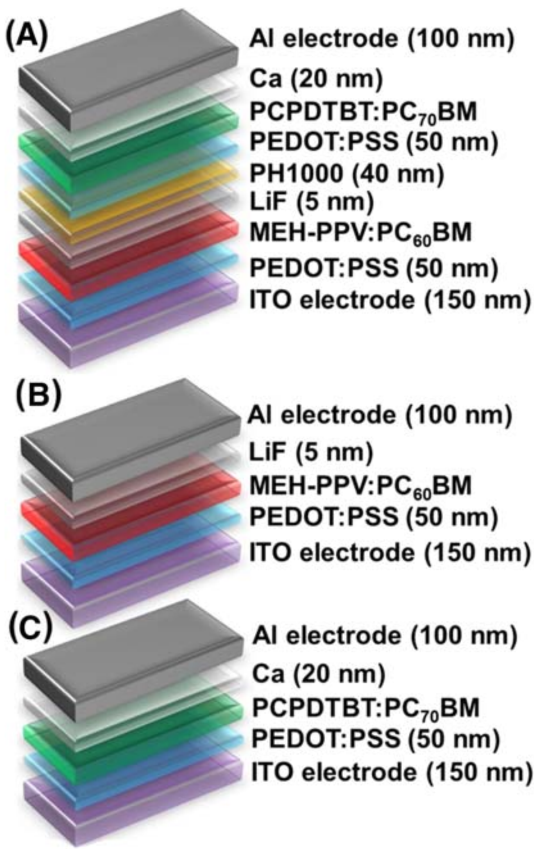

FIGURE 3 Different PV device structures constructed in FDTD software for optical simulation study. A, Tandem PV device structure constructed in FDTD software using the detailed balance model calculation for the band gap of two subcell-based monolithic tandem structure. B, Single-celled PV device structure with MEH-PPV: $PC_{60}BM$ as its active layer. C, Single-celled PV device structure with PCPDTBT:$PC_{70}BM$ as its active layer [Colour figure can be viewed at wileyonlinelibrary.com]

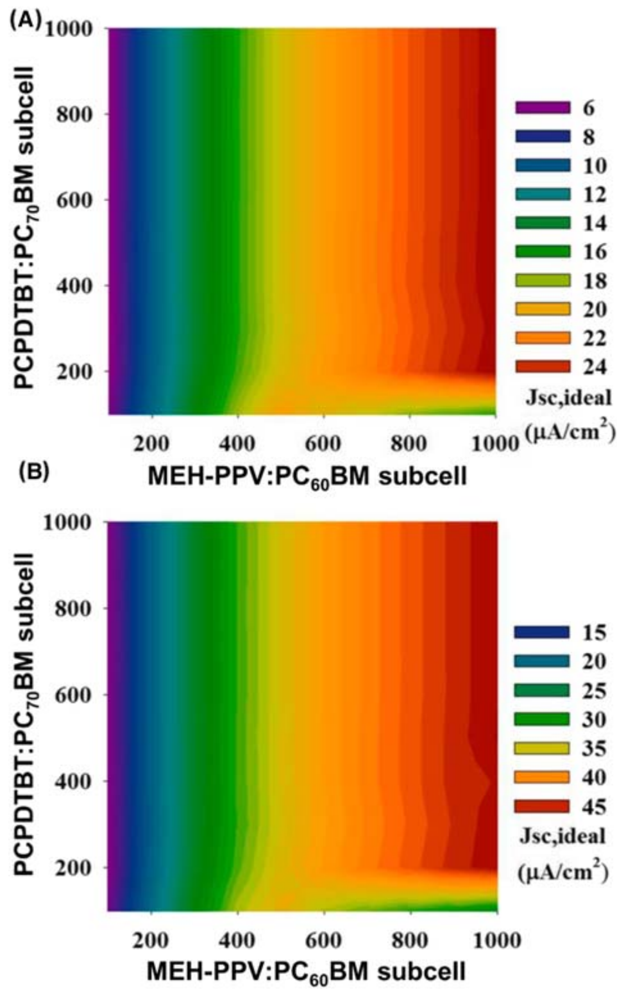

FIGURE 4 The $J_{SC,ideal}$ extracted for various combinations of active layer (MEH-PPV:$PC_{60}BM$) thickness of front subcell and active layer (PCPDTBT:$PC_{70}BM$) thickness of back subcell of the tandem structured PV device. A, $J_{SC,ideal}$ of the tandem PV cell under 500lx white LED illumination. B, $J_{SC,ideal}$ of the tandem PV cell under 1000lx white LED illumination [Colour figure can be viewed at wileyonlinelibrary.com]

one used in this work, requires current matching between the two subcells owing to Kirchhoff's law. Thus, the maximum ideal short-circuit current density ($J_{SC,max}$) will be obtained if the two subcells absorb photon flux equally, providing equal current under the 100% IQE condition assumed for the optical simulation. The $J_{SC,ideal}$ of the tandem PV cell should be a function of the subcell active layer thickness. Therefore, we simulated the tandem PV device structure with varying subcell active layer thickness. Figure 4 demonstrates that, the thickness of the front subcell active layer needs to be larger than that of the back subcell in this device structure in order to maximize $J_{SC,ideal}$. Furthermore, $J_{SC,ideal}$ is limited by the back subcell current produced by photon absorption when the back subcell thickness is less than 250 nm, and it is limited by the front subcell when the back subcell thickness is greater than 250 nm. Thus, for any back subcell active layer thickness greater than 250 nm, $J_{SC,ideal}$ is solely dependent on the front subcell photo-absorption. We simulated single-celled PV devices corresponding to each subcell in order to compare their $J_{SC,ideal}$ with that of the tandem device. The variation of $J_{SC,ideal}$ of the single-celled PV devices with the active layer thickness is depicted in Figure 5, which shows that the single active layer devices have higher $J_{SC,ideal}$ than the tandem device. This phenomenon is also observed in our experimental study under both outdoor and indoor conditions. So the simulation study confirmed that a tandem device constructed with the most suitable active materials (according to band gap matching) and optimized thickness has a lower $J_{SC,ideal}$ than that of single-celled PV devices. In order to elucidate the main cause of this phenomenon, we first estimated the absorption coefficient (α) (Figure 6B) of the active materials within the wavelength range of 300 nm –800 nm using the expression (Equation 3):

$$\alpha = \frac{4\pi k}{\lambda}, \tag{3}$$

where k is the extinction coefficient (Figure 6A) of the active material and λ is the wavelength of the incident light. Using this absorption

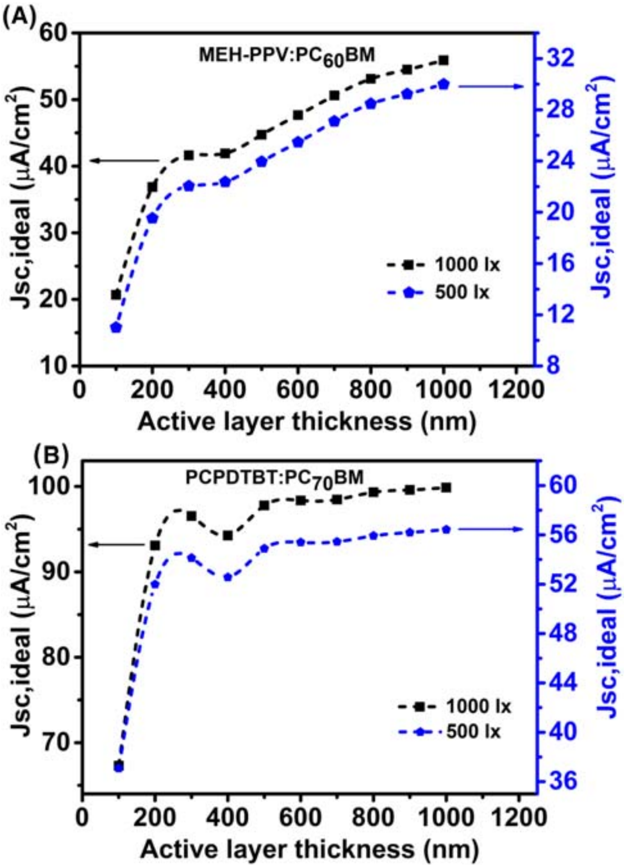

FIGURE 5 The simulated $J_{SC,ideal}$ value of PV cells containing individual active layers. A, Single-celled device with MEH-PPV: $PC_{60}BM$ as the active layer. B, Single-celled device with PCPDTBT: $PC_{70}BM$ as the active layer [Colour figure can be viewed at wileyonlinelibrary.com]

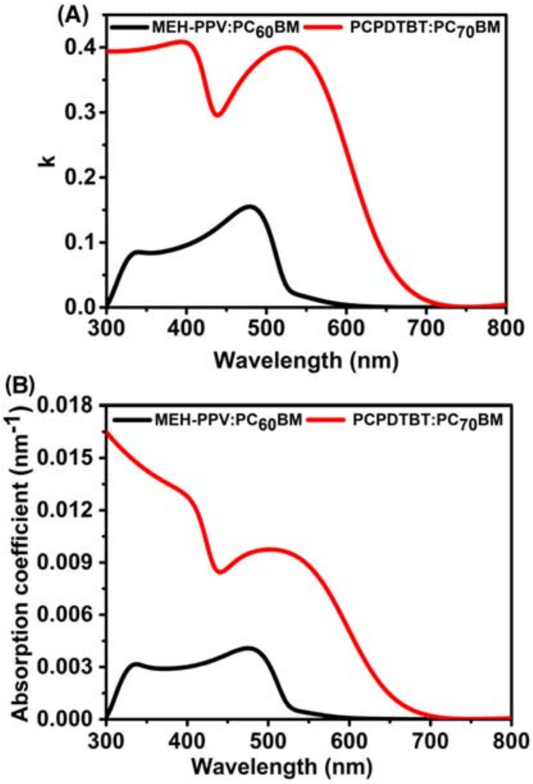

FIGURE 6 (A) The variation of the extinction coefficient of MEH-PPV:$PC_{60}BM$ and PCPDTBT:$PC_{70}BM$ with the light wavelength and (B) estimated absorption coefficient of MEH-PPV:$PC_{60}BM$ and PCPDTBT:$PC_{70}BM$ at different wavelengths [Colour figure can be viewed at wileyonlinelibrary.com]

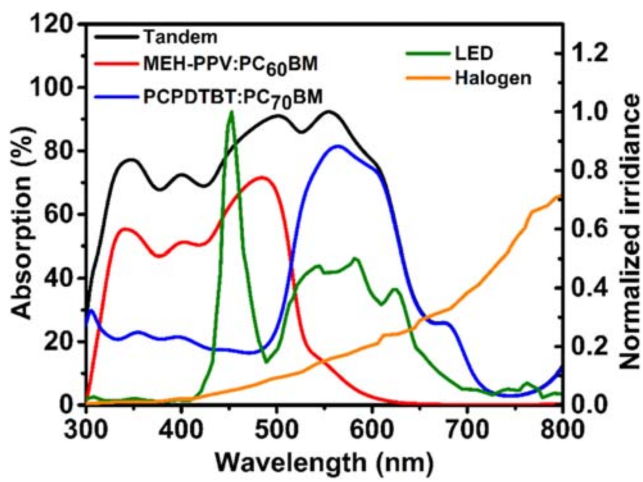

FIGURE 7 Wavelength-dependent absorption of tandem structured PV device and different single-celled PV devices and irradiance spectra of different light sources (LED and halogen) [Colour figure can be viewed at wileyonlinelibrary.com]

coefficient value, we further estimate the thickness-dependent transmission of the active materials at 450 and 550 nm. Equation 4 represents the expression of transmission as a function of absorption coefficient.

$$T = \{\exp(-\alpha \times x)\} \times 100. \tag{4}$$

where T is the transmission in % and x is the distance of the measurement point from the surface of the active layer. Figure 8A shows the transmission of 450 nm and 550 nm wavelength light through MEH-PPV:$PC_{60}BM$ and PCPDTBT:$PC_{70}BM$. We choose these two particular wavelength values as the simulated frequency-dependent absorption (%) curves (Figure 7) of MEH-PPV:$PC_{60}BM$ and PCPDTBT: $PC_{70}BM$, showing that 450 and 550 nm are the midpoints of the highest absorption regions of MEH-PPV:$PC_{60}BM$ and PCPDTBT: $PC_{70}BM$, respectively. From Figure 8A, it can be noted that PCPDTBT:$PC_{70}BM$ has a higher absorption than MEH-PPV:$PC_{60}BM$ at both wavelengths. However, at the 550nm wavelength, MEH-PPV: $PC_{60}BM$ shows a smooth descent in the transmission curve. This implies that the material does not have strong absorption near 550nm wavelength. It is a well-known fact that, the number of charge carriers generated at each point within a PV device owing to photon absorption is dependent on the absorption ability of the PV device active layer. Therefore, we further simulated the charge carrier generation rate within the tandem device at four wavelengths (450 nm, 500 nm,

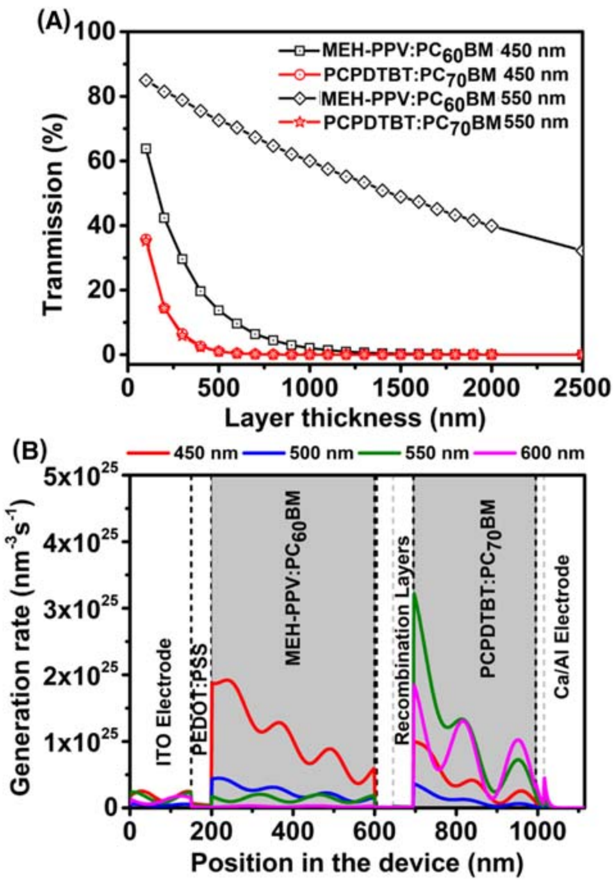

FIGURE 8 A, Thicknessdependent transmission of MEH-PPV: $PC_{60}BM$ and PCPDTBT:$PC_{70}BM$ at 450 nm and 550nm wavelengths, respectively. B, Generation rate at different positions of a tandem structured PV cell constructed with MEH-PPV:$PC_{60}BM$ as the front subcell active material and PCPDTBT:$PC_{70}BM$ as the back subcell active material [Colour figure can be viewed at wileyonlinelibrary. com]

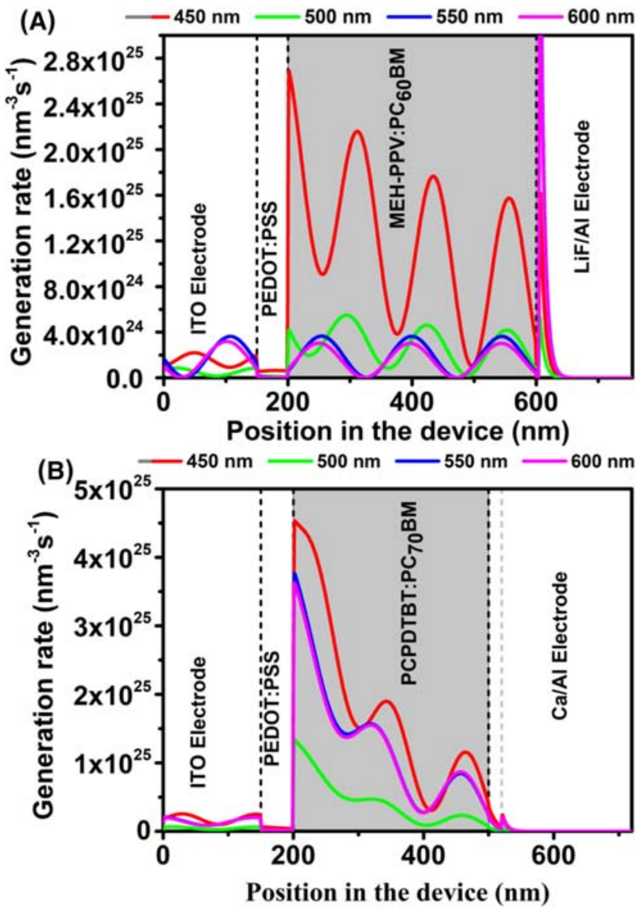

FIGURE 9 Charge carrier generation rate at different positions of a single-celled PV cell constructed with (A) MEH-PPV:$PC_{60}BM$, the active material of the front subcell, and (B) PCPDTBT:$PC_{70}BM$, the active material of the back subcell [Colour figure can be viewed at wileyonlinelibrary.com]

550 nm, and 600 nm) of incident light, as the tandem device has maximum absorption ability (Figure 7) within the wavelength range of 350 nm to 600 nm. We chose a tandem PV structure with 400nm front subcell active layer thickness and 300nm back subcell active layer thickness, considering that, we have already observed that $J_{SC,ideal}$ depends solely on the thickness of the front subcell active layer when the back subcell active layer thickness is greater than 250 nm. Figure 8B presents the charge carrier generation rate at different positions within the tandem structured PV device for incident light of wavelengths 450 nm, 500 nm, 550 nm, and 600 nm. Figure 8B illustrates that, both subcells absorb light and generate charge carriers within the tandem structured PV device for incident light with 450nm wavelength; however, for longer wavelengths (550 nm and 600 nm), the front subcell is unable to generate charge carriers owing to its low absorption coefficient value (Figure 6B). In contrast, the back subcell absorbs light energy and generates charge carriers at the longer wavelength range. Thus, the use of PCPDTBT:$PC_{70}BM$ as the back subcell and MEH PPV:$PC_{60}BM$ as the front subcell is justified. For comparison, we also simulated the distribution of the charge carrier generation rate within MEH PPV:$PC_{60}BM$ and PCPDTBT:$PC_{70}BM$-based single-celled PV cells. Figure 9 shows the photon-induced charge carrier generation rate distribution of the single-celled PV structures operating under the illumination of LED light at 450 nm, 500 nm, 550 nm, and 600nm wavelengths. It can be observed that, the charge carrier generation rates of both single-celled PV devices are higher than that of the tandem structured PV cell for LED light illumination despite the active layer band gaps of the subcells being well matched with the theoretically optimized band gap value for the particular light source. To increase the charge carrier generation rate, the number of absorbed photons should be increased. Hence, there is a correlation between the number of absorbed photons and the charge carrier generation rate in a PV cell. To support our findings regarding the charge carrier generation rate distribution within the tandem and single-celled PV devices on the basis of the distribution of the number of absorbed photons, we estimated the number of photons absorbed at different positions of the various PV devices by using the relation: $Ph_{abs} = (|E|^2 \, \mathrm{Im}(\varepsilon))/(2\hbar)$, where Ph_{abs} is the number of absorbed photons, $|E|^2$ is the simulated electric field intensity distribution within the device (Figure S1), $\mathrm{Im}(\varepsilon)$ is the imaginary part of the

permittivity (Figure S2), and ħ is the reduced Planck's constant. Figure 10A shows the number of photons absorbed in each layer of the tandem PV device. It is evident from this graph that, the back subcell absorbs most of the photons from the wavelengths under consideration. It is already observed in Figure 6B that, the absorption coefficient of the front subcell within the operating wavelength range is less than that of the back subcell. Therefore, the back subcell active layer has a very shallow skin depth compared with that of the front subcell. Hence, there is a very low possibility for a reflected photon from the back subcell to reach the front subcell. Most of the photons are absorbed by the back subcell, and thus, the front subcell generates fewer charge carriers, exhibiting a lower $J_{SC,ideal}$. This phenomenon reduces the overall current output of the tandem device. Figure 10B, C shows the number of photons absorbed by the single-celled structures shown in Figure 3B,C, respectively. The absorption of the two subcells shows that they perform better at absorbing photons when used as individual photovoltaic devices compared with when they are used in a tandem structure. Consequently, the single-celled PV cells exhibit higher $J_{SC,ideal}$ than does the tandem-structured PV cell, although the theoretically calculated band gaps are comparable with those of the active layers used to construct the tandem structured PV device. In order to maximize the $J_{SC,ideal}$ of the tandem structure, we need to enhance the current matching. To accomplish this, we have to reduce the absorption of the back subcell and increase the absorption of the front subcell in the wavelength range from 400 nm to 550 nm. Two possible options to achieve this are to increase the thickness of the front subcell active layer or to use another material with higher absorption coefficient. From Figure 8A, we know that the transmission of 450nm wavelength through MEH-PPV:PC_{60}BM drops to nearly 0% when the active layer thickness is 1000 nm. However, from Figure 4A,B, it is evident that, even at a front subcell active layer thickness of 1000 nm, the $J_{SC,ideal}$ of the tandem structured PV device is still limited by the photo-absorption of the front subcell. Moreover, increasing the thickness of the active layer or using a material with higher absorption coefficient for the front subcell will still result in lower $J_{SC,ideal}$ value of a tandem structured PV device compared with the single-celled devices, as shown in Figure 5. Thus, from this detailed simulation study, it is quite clear that, the $J_{SC,ideal}$ of a tandem structured PV cell will always be less than the $J_{SC,ideal}$ of the single-celled PV cells with the same active layers as those used to construct the tandem structured PV device. However, from Equation 2, it is evident that, the PCE value of a PV cell depends on the $J_{SC,ideal}$ and the V_{OC} values of the cell, if the FF value remains unchanged. Furthermore, from both the experimental and the simulation studies, it is clear that the $J_{SC,ideal}$ value of a tandem-structured PV device will always be less than that of the single-celled PV device, and the PCE value of the tandem PV cell is higher than that of the single-celled PV device for outdoor operation (1-sun), owing to the higher V_{OC} value (~ sum of the V_{OC} values of two subcell). However, the PCE value of a tandem cell operating under LED light is lower than that of a single-celled PV cell operating under LED light owing to the low V_{OC} value. The V_{OC} of a PV device can be expressed as

$$V_{oc} = \frac{nkT}{q} 1\text{n}\left(\frac{I_L}{I_0} + 1\right), \tag{5}$$

where n is the ideality factor which is taken as 1, k is the Boltzmann constant, T is the operating temperature, I_0 is the dark saturation current, I_L is the light-generated current, and q is the elementary charge. From Equation 5), it can be observed that the open-circuit voltage of a PV cell is logarithmically dependent on the light-generated current in the PV cell for a given temperature. Now, under the short-circuit

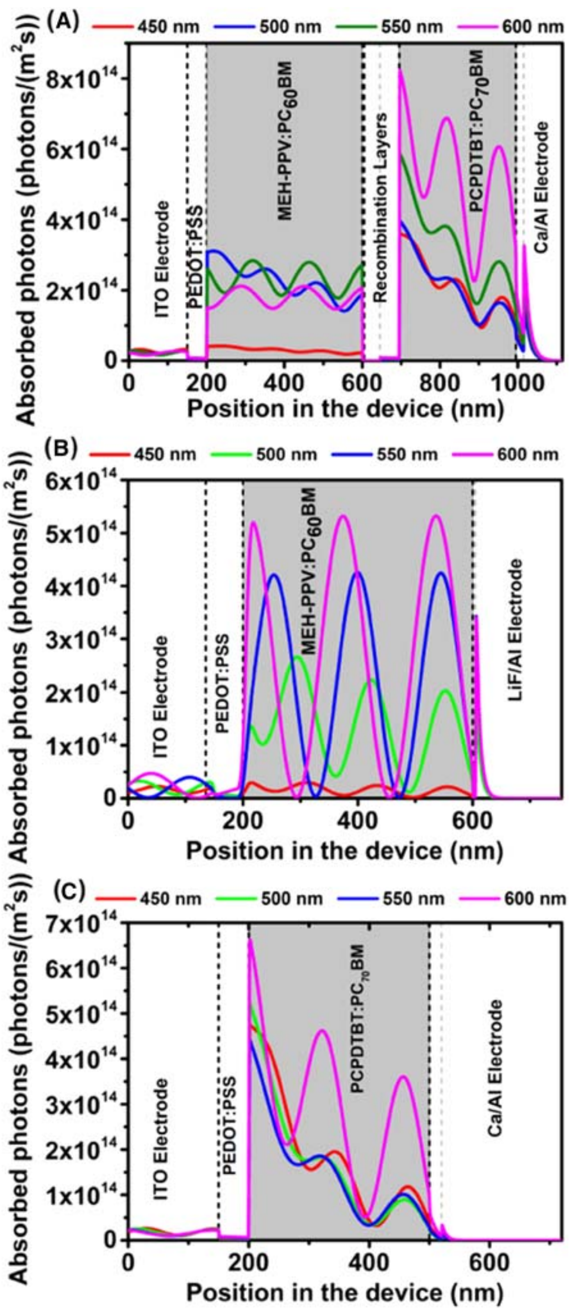

FIGURE 10 The distribution of the number of absorbed photons in each layer of (A) tandemstructured PV device, (B) MEH-PPV:PC_{60}BM-based single-celled PV device, and (C) PCPDTBT:PC_{70}BM-based single-celled PV device [Colour figure can be viewed at wileyonlinelibrary.com]

condition, the externally measured current, that is, J_{SC} is usually equal to I_L. Therefore, we can say that the V_{OC} value of a PV cell is logarithmically dependent on the J_{SC} value and dark saturation current density value of the PV cell. For low-intensity light, the J_{SC} of the tandem PV cell is reduced significantly by nearly 10^3 times. Furthermore, the effect of dark saturation current density becomes stronger. This may be the main cause for the lower value of V_{OC} obtained from the tandem structured PV cell operating under white LED light illumination.

4 | CONCLUSION

In this work, the overall performance of an organic material-based tandem structured PV cell with two subcells (P3HT:ICBA as the active layer for the front subcell and PTB7:PC_{70}BM as the active layer of the back subcell) and two single-celled PV cells with P3HT:ICBA and PTB7:PC_{70}BM as active layers was evaluated under both outdoor (1 sun) and indoor light (500- and 1000-lx white LED light) conditions. From the experimental study, it was observed that the tandem-structured PV device had a higher PCE than that of the single-celled PV cell for the 1-sun condition; however, for LED light illumination, the opposite behavior was exhibited despite the tandem-structured PV device exhibiting smaller ideal short-circuit currents for both illumination conditions. To confirm this behavior, we further conducted a detailed simulation study on a tandem structured PV cell constructed with MEH-PPV:PC_{60}BM and PCPDTBT:PC_{70}BM as the active layers of the front and back subcells, respectively, as these two materials had optimized band gaps for operating under white LED light illumination. The simulation results of the tandem photovoltaic structure were compared with the results for single BHJ structures under white LED lighting. From this simulation study it was confirmed that, a tandem-structured PV device constructed with the active materials having optimized band gaps and thicknesses would generate a smaller short-circuit current in the indoor light environment compared with a single-celled device structure. Also, for lower intensity light illumination, the dark saturation current had become more effective. Due to this phenomenon, at lower light intensity, the open-circuit voltage of the tandem PV device was reduced significantly, and the PCE of the tandem-structured PV device becomes smaller than the PCE of single-celled PV devices at low-intensity light (500 lx and 1000lx white LED) owing to the low open-circuit voltage. Therefore, it may be concluded that, a tandem-structured PV device constructed with active materials having optimized band gaps and thicknesses is not a good choice for operation under low-intensity light illumination, for example, by white LEDs.

ACKNOWLEDGEMENTS

This research was supported by the Basic Science Research Program through the NRF, funded by the Ministry of Education (NRF-2018R1D1A1B07043759/NRF-2018 R1D1A3B07049992). This research was also supported by the Technology Development Program to Solve Climate Changes of the NRF, funded by the Ministry of Science, ICT & Future Planning (NRF-2016M1A2A2940912) and Basic Science Research Program through the National Research Foundation of Korea (NRF) funded by the Ministry of Science and ICT (2018R1A2B6008815).

ORCID

Hyeok Kim https://orcid.org/0000-0003-2164-2849

REFERENCES

1. Shockley W, Queisser HJ. Detailed balance limit of efficiency of p-n junction solar cells. *J Appl Phys*. 1961;32(3):510-519.
2. Rühle S. Tabulated values of the Shockley–Queisser limit for single junction solar cells. *Sol Energy*. 2016;130:139-147.
3. Jackson P, Hariskos D, Lotter E, et al. New world record efficiency for Cu(In,Ga)Se_2 thin-film solar cells beyond 20%. *Prog Photovoltaics Res Appl*. 2011;19(7):894-897.
4. Masuko K, Shigematsu M, Hashiguchi T, et al. Achievement of more than 25% conversion efficiency with crystalline silicon heterojunction solar cell. *IEEE J Photovoltaics*. 2014;4(6):1433-1435.
5. Alharbi FH, Kais S. Theoretical limits of photovoltaics efficiency and possible improvements by intuitive approaches learned from photosynthesis and quantum coherence. *Renew Sustain Energy Rev*. 2015; 43:1073-1089.
6. Green MA, Hishikawa Y, Dunlop ED, Levi DH, Hohl-Ebinger J, Ho-Baillie AWY. Solar cell efficiency tables (version 52). *Prog Photovoltaics Res Appl*. 2018;26(7):427-436.
7. He Z, Zhong C, Su S, Xu M, Wu H, Cao Y. Enhanced power-conversion efficiency in polymer solar cells using an inverted device structure. *Nat Photonics*. 2012;6(9):591-595.
8. Scharber MC, Mühlbacher D, Koppe M, et al. Design rules for donors in bulk-heterojunction solar cells—towards 10% energy-conversion efficiency. *Adv Materials*. 2006;18(6):789-794.
9. YuanJ, Ford MJ, Xu Y, Zhang Y, Bazan GC, Ma W. Improved tandem all-polymer solar cells performance by using spectrally matched subcells. *Adv Energy Mater*. 2018;8(14):1703291.
10. Meng L, Zhang Y, Wan X, et al. Organic and solution-processed tandem solar cells with 17.3% efficiency. *Science*. 2018;361:1094-1098.
11. Ameri T, Li N, Brabec CJ. Highly efficient organic tandem solar cells: a follow up review. *Energ Environ Sci*. 2013;6(8):2390-2413.
12. Roundy S, Steingart D, Frechette L, Wright P, Rabaey J. Power sources for wireless sensor networks. *European Workshop on Wireless Sensor Networks, Springer*. 2004;1-17.
13. Warneke BA, Scott MD, Leibowitz BS, et al. An autonomous 16 mm/-sup 3/solar-powered node for distributed wireless sensor networks. *Sensors, 2002 IEEE*. 2002;1510-1515.
14. Hande A, Polk T, Walker W, Bhatia D. Indoor solar energy harvesting for sensor network router nodes. *Microprocess Microsys*. 2007;31(6): 420-432.
15. Tan YK, Panda SK. Energy harvesting from hybrid indoor ambient light and thermal energy sources for enhanced performance of wireless sensor nodes. *IEEE Trans Ind Electron*. 2011;58(9):4424-4435.
16. Águas H, Mateus T, Vicente A, et al. Thin film silicon photovoltaic cells on paper for flexible indoor applications. *Adv Funct Mater*. 2015;25 (23):3592-3598.
17. Shin SC, Koh CW, Vincent P, et al. Ultra-thick semi-crystalline photoactive donor polymer for efficient indoor organic photovoltaics. *Nano Energy*. 2019;58:466-475.
18. Mathews I, King PJ, Stafford F, Frizzell R. Performance of III–V solar cells as indoor light energy harvesters. *IEEE J Photovolt*. 2016;6(1): 230-235.
19. TingareYS, Vinh NSN, Chou HH, et al. New acetylene-bridged 9, 10-conjugated anthracene sensitizers: application in outdoor and indoor dye-sensitized solar cells. *Advanced Energy Materials*. 2017;7: 1700032.

20. Deline C, Stokes A, Silverman T J, Rummel S, Jordan D, Kurtz S. Electrical bias as an alternate method for reproducible measurement of copper indium gallium diselenide (CIGS) photovoltaic modules. Reliability of Photovoltaic Cells, Modules, Components, and Systems V, International Society for Optics and Photonics. 2012:84720G. https://www.spiedigitallibrary.org/conference-proceedings-of-spie/8472/84720G/Electrical-bias-as-an-alternate-method-for-reproducible-measurement-of/10.1117/12.929899.short
21. Lucarelli G, Di Giacomo F, Zardetto V, Creatore M, Brown TM. Efficient light harvesting from flexible perovskite solar cells under indoor white light-emitting diode illumination. *Nano Res*. 2017;10(6):2130-2145.
22. Minnaert B, Veelaert P. A proposal for typical artificial light sources for the characterization of indoor photovoltaic applications. *Energies*. 2014;7(3):1500-1516.
23. Minnaert B, Veelaert P. The potential of tandem photovoltaic solar cells for indoor applications. 1st International e-Conference on Energies, Sciforum Electronic Conference Series. 2014.
24. De Vos A. Detailed balance limit of the efficiency of tandem solar cells. *Journal of Physics D*. 1980;13(5):839-846.
25. Vincent P, Shin SC, Goo JS, et al. Indoor-type photovoltaics with organic solar cells through optimal design. *Dyes and Pigments*. 2018; 159:306-313.
26. Duche D, Torchio P, Escoubas L, et al. Improving light absorption in organic solar cells by plasmonic contribution. *Sol Energy Mater sol Cells*. 2009;93(8):1377-1382.
27. Zhu J, Zeng B, Kim R S, Wu Z. Light concentration in polymer bulk heterojunction solar cells with plasmonic nanoparticles. Photonics and Optoelectronics Meetings (POEM) 2011: Optoelectronic devices and integration, International Society for Optics and Photonics 2012: 83331C. https://www.spiedigitallibrary.org/conference-proceedings-of-spie/8333/83331C/Light-concentration-in-polymer-bulk-heterojunction-solar-cells-with-plasmonic/10.1117/12.914545.short?SSO=1
28. Chen CC, Chang WH, Yoshimura K, et al. An efficient triple-junction polymer solar cell having a power conversion efficiency exceeding 11%. *Adv Mater*. 2014;26(32):5670-5677.

SUPPORTING INFORMATION

Additional supporting information may be found online in the Supporting Information section at the end of this article.

How to cite this article: Biswas S, You Y-J, Vincent P, Bae J-H, Shim JW, Kim H. Organic tandem solar cells under indoor light illumination. *Prog Photovolt Res Appl*. 2020;28:946–955. https://doi.org/10.1002/pip.3301